JACS
JOURNAL OF THE AMERICAN CHEMICAL SOCIETY

Communication

pubs.acs.org/JACS

Hexaaminobenzene as a building block for a Family of 2D Coordination Polymers

Nabajit Lahiri,[†] Neda Lotfizadeh,[‡] Ryuichi Tsuchikawa,[‡] Vikram V. Deshpande,*[,‡] and Janis Louie*[,†]

[†]Department of Chemistry and [‡]Department of Physics and Astronomy, University of Utah, Salt Lake City, Utah 84112, United States

Supporting Information

ABSTRACT: A family of 2D coordination polymers were successfully synthesized through "bottom-up" techniques using Ni^{2+}, Cu^{2+}, Co^{2+}, and hexaaminobenzene. Liquid−liquid and air−liquid interfacial reactions were used to realize thick (~1−2 μm) and thin (<10 nm) stacked layers of nanosheet, respectively. Atomic-force microscopy and scanning electron microscopy both revealed the smooth and flat nature of the nanosheets. Selected area diffraction was used to elucidate the hexagonal crystal structure of the framework. Electronic devices were fabricated on thin samples of the Ni analogue and they were found to be mildly conducting and also showed back gate dependent conductance.

Graphene, an atomically thin π-conjugated 2D organic polymer, is the strongest material to date and also an extraordinary conductor of heat and electricity. The extraordinary physical properties of graphene have been utilized in various applications such as electronics,[1−3] spintronics,[4,5] solar cells,[6,7] and batteries.[8] However, graphene is just one member of a wider class of 2D materials, some of which possess additional functionalities such as semiconducting band gap, superconductivity, magnetism, and topological order. Thus far, the major graphene alternatives are 2D transition-metal chalcogenides, which are locked by their constituent elements and are difficult to modify by design. A "bottom-up" approach to 2D materials, on the other hand, allows one to tailor material properties by design. In this context, 2D coordination polymers (CPs), which can be synthesized via judicious selection of metal centers and coordinating ligands, are of particular interest due to their high tunability.

Currently, only a limited number of syntheses of two-dimensional CPs have been reported.[9−17] Moreover, the resultant 2D CPs are usually either multilayered with thickness greater than 300 nm or are polycrystalline with submicrometer sized crystallites. Such characteristics make them unsuitable for advanced device fabrication which requires single (or few) layered π-conjugated CPs that have large lateral dimensions (μm^2 or mm^2). As such, the synthesis of few-layered (<10 layers) 2D CPs still remains to be a formidable challenge.[12−14] Herein we report the synthesis of a family of 2D CPs that are not only large in lateral dimension (μm^2) but also ultrathin (<10 nm) and crystalline. Using hexaaminobenzene as the coordinating ligand and metal ions such as Ni^{2+}, Cu^{2+}, and Co^{2+} as the metal linkers, we have prepared several nitrogen-based few-layered CPs.

A gas−liquid interfacial reaction was used wherein hexaaminobenzene (HAB) was dissolved in degassed, deionized water, and an ethyl acetate solution of $M(acac)_2$ (M = Ni, Cu, Co, acac = acetylacetonate) was gently added on top of the aqueous phase such that it covered approximately half of the surface (Figure 1). The reaction was allowed to sit for 4 h to allow for the ethyl acetate to evaporate. The 2D (hexaiminobenzosemiquinonato)-κN-metal complex (**1**) could be seen to form spontaneously as a film on the surface. The thin films were then transferred to suitable substrates (e.g., SiO_2 (300 nm)/Si, polydimethylsiloxane (PDMS) gel, etc.) using a Langmuir−Schafer type of extraction that involves the gentle lowering of the substrates face-down onto the surface of the reaction mixture and then lifting it up. After washing with water and isopropyl alcohol, the substrate adhered CPs were

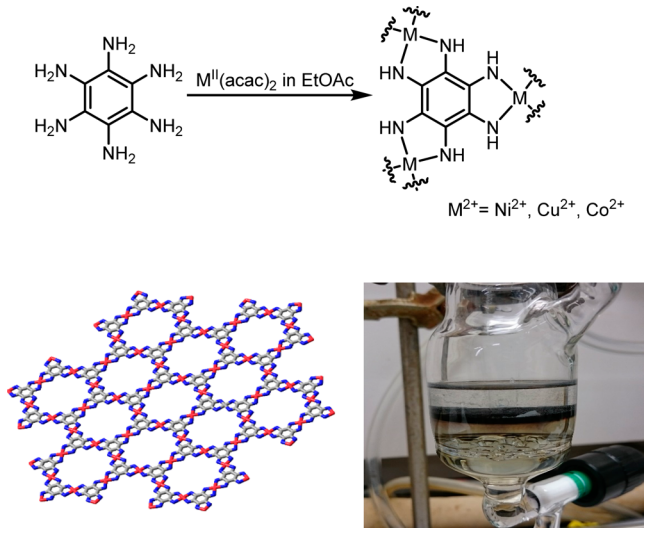

Figure 1. (Top) General synthesis of CPs. (Bottom) Schematic illustration of the structure of the nanosheet (tube model with hydrogens omitted for clarity: Gray, carbon; blue, nitrogen; red, metal ion) and photograph of the reaction vessel highlighting the liquid/liquid (EtOAc−water) interfacial synthesis of Ni-HAB complex showing the polymer as a black solid at the interface.

Received: September 20, 2016
Published: December 12, 2016

DOI: 10.1021/jacs.6b09889
J. Am. Chem. Soc. 2017, 139, 19−22

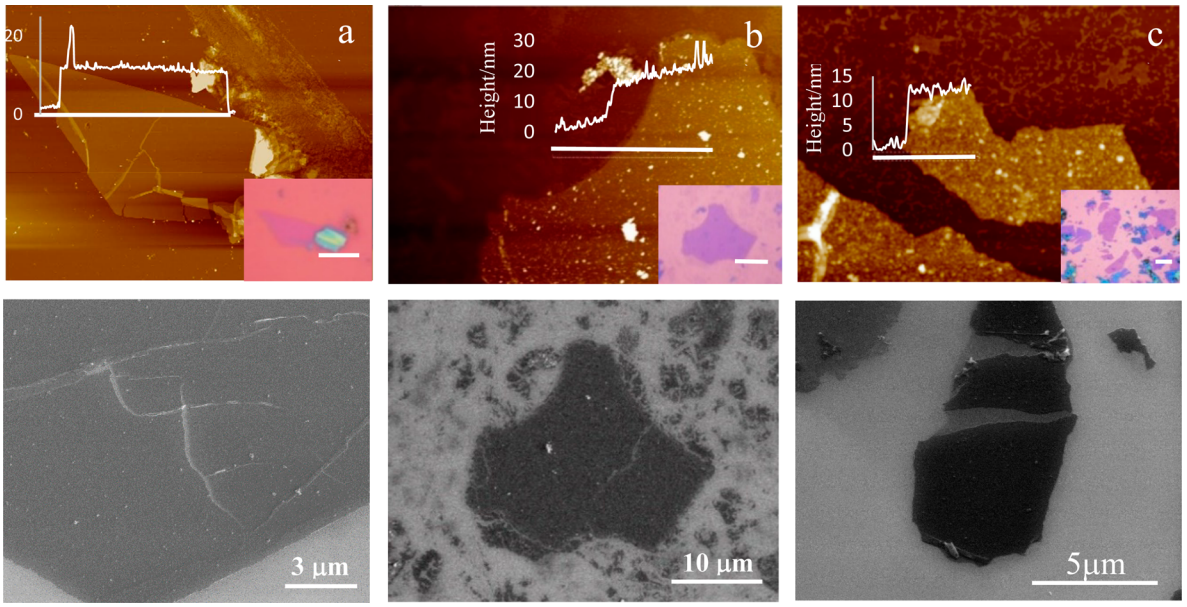

Figure 2. Characterization of 2D-CPs. (a) (Top) AFM height profile image of **1-Ni** on SiO_2 (300 nm)/Si substrate with OM image in inset; (bottom) SEM image of **1-Ni**. (b) (Top) AFM height profile image of **1-Cu** on SiO_2 (300 nm)/Si substrate with OM image in inset; (bottom) SEM image of **1-Cu**. (c) (Top) AFM height profile image of **1-Co** on SiO_2 (300 nm)/Si substrate with OM image in inset; (bottom) SEM image of **1-Co**. All OM image scale bars are equivalent to 10 μm.

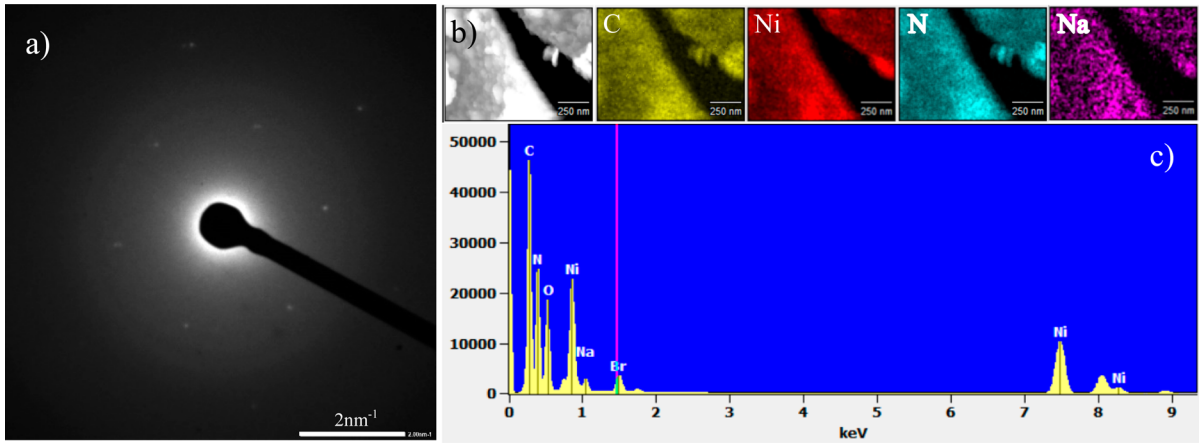

Figure 3. Transmission electron microscope images of **2-Ni**. (a) Selected-area diffraction (SAED) on the nanosheet **2-Ni** showing a hexagonal lattice (scale bar: 2 nm^{-1}). (b) Secondary electron image of **2-Ni** using TEM, brighter regions indicate the film, whereas darker regions the carbon film support and elemental mapping images of carbon, nitrogen, nickel, and sodium using S/TEM-EDS. (c) EDS of the corresponding area of **2-Ni** where SAED was performed showing the elemental composition.

subjected to sonication in EtOAc for 10 s followed by baking at 100 °C under a dynamic vacuum for 12 h.

Analysis of the 2D CPs on 300 nm SiO_2/Si with optical microscopy (OM) and scanning electron microscopy (SEM) confirmed the CPs were homogeneous and crystalline films that generally lacked cracks over fairly large areas (Figure 2). Furthermore, atomic-force microscopy (AFM) profilometry of Ni-HAB (**1-Ni**), Cu-HAB (**1-Cu**), and Co-HAB (**1-Co**) showed that the family of 2D-CPs had similar thicknesses of ~10 nm (10, 11, and 13 nm, respectively, Figure 2), which corresponds to about 8−10 monolayers of the respective 2D-CPs stacked on one another. A single layer of fairly large dimensions, however, could not be obtained possibly due to strong π-stacking interactions between layers.

The composition of the respective 2D CPs films was examined by X-ray photoelectron spectroscopy (XPS). Importantly, XPS of each 2D CP confirmed only presence of the carbon, nitrogen, and expected transition metal (i.e., Ni, Cu, or Co) as well as sodium, the counterion used during syntheses (Figures S1, S8, and S14). In the Ni-HAB complex (**1-Ni**), a high-resolution scan of the Ni (2p) region showed the presence of Ni^{2+} in the complex (Figure S2). Furthermore, deconvolution of the N (1s) region in **1-Ni** reveals the presence of three distinct N (1s) peaks (Figure S4). The peak at 400 eV corresponds to adventitious nitrogen that is physically adsorbed on the surface. The peaks at ~399 and ~398 eV were attributed to nitrogen at "0" and "−1" oxidation states respectively which were present in a 42:58 ratio (Table T1). In other words, the Ni-HAB complex (**1-Ni**) had a net negative charge that was balanced by the presence of Na^+ counterions. Similar results were obtained for the **1-Cu** and **1-Co** analogues. The Cu-HAB complex was found to only have peaks corresponding to

DOI: 10.1021/jacs.6b09889
J. Am. Chem. Soc. 2017, 139, 19−22

copper, carbon, and nitrogen (Figure S8). A high resolution scan in the Cu (2p) region, however, revealed the presence of a mixture of Cu^{2+} and Cu^{+} species. Such mixed valencies have been previously observed in copper complexes and can be attributed to the redox-active nature of the ligand.[9] Similarly, the Co (2p) region of the Co-HAB complex was found to consist of two sets of peaks (Figure S15). The first set was at 780 and 796 eV; the second set was at 785 and 802 eV. These were attributed to Co^{2+} and Co^{3+} species, respectively. Interestingly, the Cu-HAB (**1-Cu**) and the Co-HAB (**1-Co**) were found to be neutral as supported by the absence of Na^{+} ions in the XPS spectra of the complexes.

To investigate further the internal structure and crystallinity of these 2D CPs, selected area diffraction (SAED) was performed on **2-Ni** using TEM. Ultrathin films (<10 nm) of **1-Ni** could not be used for TEM studies due to extensive radiolysis damage. Analysis of a thick film (**2-Ni**, ca. 1 μm) that was synthesized using a liquid/liquid interfacial reaction (see SI for details) displayed the expected hexagonal diffraction pattern, thus confirming the Ni-HAB complex was crystalline in nature with a hexagonal lattice (Figure 3). The lattice spacing was determined to be 0.5 nm. Similar hexagonal diffraction patterns were also observed for both Cu-HAB (**2-Cu**) and Co-HAB complexes (**2-Co**), which had *d*-spacings of 0.40 and 0.43 nm, respectively (Figures S12 and S18). Additionally, the atom-ratio of nickel to nitrogen obtained from S/TEM-EDS (EDS, energy-dispersive spectroscopy) of **2-Ni** spectra was close to 1:4 and supports the proposed structure. Elemental mapping on the complexes also revealed a homogeneous distribution of carbon, nitrogen, and the respective metal on the nanosheet (Figures 3b, S12, and S18).

Nanosheets were electrically characterized by fabricating devices using either direct transfer on prefabricated leads, shadow mask lithography, or electron-beam lithography. Using the first procedure results in bottom contacts (Figure 4a) and yields top contacts (Figure 4a) with the other two procedures.

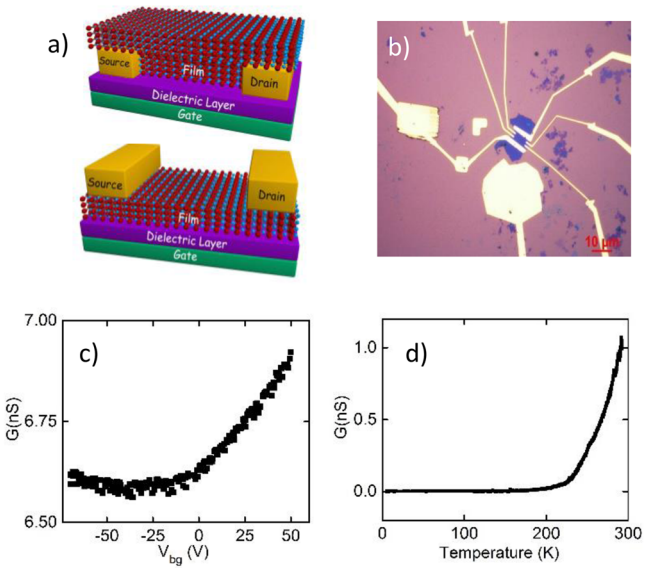

Figure 4. Electrical characterization of **1-Ni**. (a) (Top) Top contact and (bottom) bottom contact scheme of electrical contacts. (b) Typical top-contact device architecture using e-beam lithography. (c) Back gate V_{bg} dependent conductance of **1-Ni** (20 nm). (d) Temperature dependent conductance of **2-Ni**.

In all three cases, devices were similarly resistive, in the GΩ range, and showed slight modulation of conductance *G* with respect to variation of a back gate voltage V_{bg}. Figure 4c shows a typical gate-dependent conductance of a Ni nanosheet device. Finally, Figure 4d shows the temperature dependent conductance of a different Ni nanosheet device down to 4 K from room temperature. In general, devices tended to decrease in conductance as temperature was lowered indicating insulating behavior in charge transport.

In conclusion, we synthesized a family of hexaaminobenzene based Coordination Polymers (CPs) having a hexagonal honeycomb crystal lattice. The morphology, composition, and crystal structure of the complexes were confirmed by OM, FE-SEM, AFM, XPS, and S/TEM. Both top and bottom contacts used for electrical characterizations yielded similar values of resistances. We attribute the low conductivity of the samples to the low crystallinity of the framework resulting in crystal defects and grain boundaries. Efforts toward the synthesis of samples with lower defects by optimizing reaction conditions and fabrication techniques are currently underway.

■ ASSOCIATED CONTENT

Supporting Information

The Supporting Information is available free of charge on the ACS Publications website at DOI: 10.1021/jacs.6b09889.

Experimental details, FE-SEM, HR-TEM, SAED, XPS, S/TEM-EDS data, and electrical characterization data (PDF)

■ AUTHOR INFORMATION

Corresponding Authors

*J.L. louie@chem.utah.edu
*V.V.D. vikramvd@gmail.com

ORCID

Janis Louie: 0000-0003-3569-1967

Notes

The authors declare no competing financial interest.

■ ACKNOWLEDGMENTS

This work was supported by the National Science Foundation MRSEC program at the University of Utah under grant #DMR 1121252. We gratefully acknowledge Brian van Devener and Paulo Perez for help with TEM data. We also gratefully acknowledge Jonathan David Ogle for assistance with Raman data and Emily Fullwood for help with acquiring TGA data.

■ REFERENCES

(1) Geim, A. K.; Novoselov, K. S. *Nat. Mater.* **2007**, *6*, 183.
(2) Lin, Y. M.; Dimitrakopoulos, C.; Jenkins, K. A.; Farmer, D. B.; Chiu, H. Y.; Grill, A.; Avouris, P. *Science* **2010**, *327*, 662.
(3) Novoselov, K. S.; Geim, A. K.; Morozov, S. V.; Jiang, D.; Zhang, Y.; Dubonos, S. V.; Grigorieva, I. V.; Firsov, A. A. *Science* **2004**, *306*, 666.
(4) Maassen, J.; Ji, W.; Guo, H. *Nano Lett.* **2011**, *11*, 151.
(5) Son, Y.-W.; Cohen, M. L.; Louie, S. G. *Nature* **2006**, *444*, 347.
(6) Miao, X.; Tongay, S.; Petterson, M. K.; Berke, K.; Rinzler, A. G.; Appleton, B. R.; Hebard, A. F. *Nano Lett.* **2012**, *12*, 2745.
(7) Wang, X.; Zhi, L.; Müllen, K. *Nano Lett.* **2008**, *8*, 323.
(8) Liu, Y.; Artyukhov, V. I.; Liu, M.; Harutyunyan, A. R.; Yakobson, B. I. *J. Phys. Chem. Lett.* **2013**, *4*, 1737.
(9) Campbell, M. G.; Sheberla, D.; Liu, S. F.; Swager, T. M.; Dinca, M. *Angew. Chem., Int. Ed.* **2015**, *54*, 4349.

DOI: 10.1021/jacs.6b09889
J. Am. Chem. Soc. 2017, 139, 19−22

(10) Clough, A. J.; Yoo, J. W.; Mecklenburg, M. H.; Marinescu, S. C. *J. Am. Chem. Soc.* **2015**, *137*, 118.
(11) Huang, X.; Sheng, P.; Tu, Z.; Zhang, F.; Wang, J.; Geng, H.; Zou, Y.; Di, C.-a.; Yi, Y.; Sun, Y.; Xu, W.; Zhu, D. *Nat. Commun.* **2015**, *6*, 7408.
(12) Kambe, T.; Sakamoto, R.; Hoshiko, K.; Takada, K.; Miyachi, M.; Ryu, J.-H.; Sasaki, S.; Kim, J.; Nakazato, K.; Takata, M.; Nishihara, H. *J. Am. Chem. Soc.* **2013**, *135*, 2462.
(13) Pal, T.; Kambe, T.; Kusamoto, T.; Foo, M. L.; Matsuoka, R.; Sakamoto, R.; Nishihara, H. *ChemPlusChem* **2015**, *80*, 1255.
(14) Sakamoto, R.; Hoshiko, K.; Liu, Q.; Yagi, T.; Nagayama, T.; Kusaka, S.; Tsuchiya, M.; Kitagawa, Y.; Wong, W.-Y.; Nishihara, H. *Nat. Commun.* **2015**, *6*, 6713.
(15) Sheberla, D.; Sun, L.; Blood-Forsythe, M. A.; Er, S.; Wade, C. R.; Brozek, C. K.; Aspuru-Guzik, A.; Dinca, M. *J. Am. Chem. Soc.* **2014**, *136*, 8859.
(16) Dong, R.; Pfeffermann, M.; Liang, H.; Zheng, Z.; Zhu, X.; Zhang, J.; Feng, X. *Angew. Chem., Int. Ed.* **2015**, *54*, 12058.
(17) Dong, R.; Pfeffermann, M.; Liang, H.; Zheng, Z.; Zhu, X.; Zhang, J.; Feng, X. *Angew. Chem., Int. Ed.* **2015**, *54*, 12058.

DOI: 10.1021/jacs.6b09889
J. Am. Chem. Soc. 2017, 139, 19−22